Optimum operational planning of wind-integrated power systems with embedded Multi-terminal High Voltage Direct Current Links using the Flexible Universal Branch Model

1st Siti Khadijah Hamzah
dept. of Engineering
Durham University
Durham, United Kingdom
siti.k.hamzah@durham.ac.uk

2nd Behzad Kazemtabrizi
dept. of Engineering
Durham University
Durham, United Kingdom
behzad.kazemtabrizi@durham.ac.uk

***Abstract*—This paper presents a comprehensive analysis of a meshed MT-HVDC topology with three wind farms connected to the Substation Ring Topology (SRT) and investigates the steady state performance of the MT-HVDC system based on the VSC control strategies (i.e. conventional method and droop control), which was modelled via the FUBM model and produced results that is useful for solving Optimal Power Flow, particularly in the systems where hybrid AC/DC are adopted to integrate with the large-scale wind resources. The main focus is on the impact evaluation of various VSC control strategies. The outcome indicated that the VSC based MT-HVDC system performs well in terms of power transmission stability and reliability. The operational gain of the simulation results is that the Electricity system operator has the preference for the most robust strategy for the operational planning depending on the system requirements.**

***Index Terms*—VSC control strategies, MT-HVDC, FUBM, Optimal Power Flow, mesh network, wind farms**

I. Introduction

The development of the High Voltage Direct Current system has been driven by: a) the escalating need for electrical power on a global scale; b) the optimal utilisation of transmission lines; and c) the operational flexibility [1]. A Multi-Terminal High Voltage Direct Current (MT-HVDC) system, a recent development in the HVDC innovation, is presented for the integration of the large wind farms' captured energy into an onshore Alternating Current (AC) grid in the future. This system comprises of several converters that are connected either in radial or meshed DC networks [2]. Renewable energy sources like wind farms generate electricity that can be transported to the grid via submarine Direct Current (DC) cables, which makes them an appealing technology and ideal for creating an interconnected DC network hub for maximising renewable resource sharing. MT-HVDC interconnectors can also be used to facilitate transmission of electrical energy over long distances and across international borders thereby creating a global interconnected network. A precursor of this has already been studied extensively in the context of the European Supergrid (ES) [3, 4].

The MT-HVDC links focused in this paper are based on the Voltage Source Converter (VSC) technology. VSCs allow for a controlled AC voltage synthesis from a fixed DC input voltage source using fast switching of Insulated Gate Bipolar Junction Transistors (IGBTs). This feature enables VSCs to control individually the magnitude (i.e. amplitude) and the phase angle of the AC voltage at their output terminals [5], which in turn allows the converter to control, independently, active and reactive power output making them ideal to be connected to weak AC networks and for bulk integration of variable output of renewable energy resources. The additional operational flexibility promised by VSCs (i.e., independent active/reactive power control and AC voltage control) are crucial for the grid network operation especially for systems with high levels of variable renewable resources integrated [6]. In general, the VSC-HVDC systems has the following benefits when compared to the current source converter variants: (i) they have a smaller footprint because they require smaller filters; (ii) they are capable of performing black starts; (iii) they allow for controllable and flexible power flow; and (iv) they are capable of connecting and energising weak AC grids [3, 7]. These advantages enable the realisation of the large-scale offshore transmission grids, such as ES and North Sea Wind Farms (NSWF). Both concepts could be implemented through the use of VSC-based MT-HVDC topologies.

The Optimal Power Flow (OPF) problem is a mathematical optimisation problem that is normally solved by the Electricity System Operator (ESO) to identify an economic resource dispatch schedule ahead of real-time operation based on network's realistic operational constraints (i.e., nodal voltage magnitudes and real and reactive power limits in transmission lines) [8, 9]. The OPF problem that is normally solved in this context is useful for identifying any control actions, by generators, transformers, and any other available control devices in the system under both normal and abnormal operating conditions. The ESO therefore solves instances of OPF problems to account for any changes in the system's steady-state

operating points (generators' resource dispatch, transformers' tap changer positions, and other controller actions) to *plan* the system operation in a reliable and economic manner ahead of real-time operation. Yet, developing accurate models that are capable of representing the control actions of VSC converters, especially in the context of operating in a meshed MT-HVDC network is still an area of active research [10, 11].

Presently, the standard PF and the OPF formulations are only suited for AC systems [8]. Moreover, most software implementation of PF/OPF solvers lack the model libraries [12] and realistic network element representations required for implementing and solving a system with embedded VSC-HVDC links and their associated controls (voltage and power control), to provide a quick and an accurate solution for hybrid AC/DC networks. Besides that, existing OPF formulations mostly employ a sequential methodology to independently solve the AC and DC elements of the hybrid networks. As a result, the governing equations for each model (AC and DC) are different [10].

In this research, the focus will be on using the new Flexible Universal Branch Model (FUBM) first developed by Bustos, et. al in [13, 10]. The scalability of this model had been established by the authors above, which showed that it can efficiently solve the hybrid AC/DC network within a single frame of reference (i.e., all equations for all system elements are effectively similar and the whole system is notionally modelled as an AC system). Furthermore, the model maintains numerical solution (i.e. computational tractability) for larger system without degrading convergence time. The attractiveness of this model is that it can be readily used to solve PF/OPF for systems with embedded VSC-HVDC links (like the ones presented in this paper) taking into account additional control variables/constraints that represent the control characteristics of the VSCs (i.e.,voltage and power flow control) [14].

In this paper, all network elements are therefore modelled using the FUBM for purposes of solving OPF. The main contributions of this paper is therefore in establishing a new modelling framework for modelling and incorporating additional control actions of VSC converters for steady-state operational planning of meshed MT-HVDC networks. These networks are crucial for large-scale variable wind resource integration and it is thus essential for the ESO to have the ability to schedule control actions promised by individual VSC terminals when planning network operation in wind-integrated power systems of the future. The control actions in turn provide the ESO with the additional levels of flexibility required for operating such networks in a reliable manner and allowing for maximisation of the utilisation of the variable wind resource reliably. For clarity, in this paper a meshed network topology has been chosen [15].

The rest of the paper is as follows: Section II gives a brief overview of VSC control strategies (conventional and droop) before explaining how these control strategies are implemented in a steady-state planning framework using the Flexible Universal Branch Model (FUBM), Section III gives a comprehensive overview of the mathematical model formulation of FUBM and the ensuing OPF with all VSC control strategies incorporated, finally in Section IV, a set of results are analysed for a modified test system with a meshed MT-DC link used to integrate three wind farms to an asynchronous AC network.

II. VSC-MTHVDC CONTROL STRATEGIES

Voltage and power regulation within an MT-HVDC grid has been challenging due to the large number of stations, with the ultimate goal of generating a desired power flow in the grid[16]. The MT-HVDC performance is highly dependent on the control technique used, which is primarily based on an AC grid connection and the architecture of the dc network [17]. In [18], the authors have identified several types of power control strategies that have been implemented in the current MT-HVDC systems, which include main-follower control, margin voltage control, priority control, ration control and droop control. In their research, a main-follower control technique for AC/DC connections had been implemented in their case study, which identifies one DC bus as a slack node.

The VSC-MTHVDC employs two different types of control strategies: traditional control typically regulates the DC voltage and active power, and the droop control which is a generalisation of the traditional approach [19]. Both methods have been mathematically incorporated into the FUBM to resolve the OPF problem for the MT-HVDC system [10]. Further discussion on the FUBM's control strategy is provided in sub-section II-C.

A. Conventional method

A classical control strategy for the VSC-MTDC system can be divided to a DC voltage and active power. Based on research [19], the most straightforward control strategy is the DC voltage control, which sets one VSC for continuous voltage control and the other VSCs for constant power control. The voltage controlled VSC maintains the power balance of the entire DC grid. In [20] this form of control is called a main-follower (also known as a master slave) control that assigned a single VSC to control the DC voltage, whilst other VSCs are responsible of regulating the injected power into the AC grids. According to [21] this form of control is crucial for ensuring the efficient operation of the MT-HVDC link, since it shows the system's inherent power balance and stability. [11] indicated that the function of the master converter (i.e. slack VSC) is to deliver or absorb any power imbalances in the DC network. Thus, the availability and capabilities of this converter are fundamental to the power balance in the MT-HVDC link. The second type of traditional control is an active power control, which is likewise the simplest technique similar to the DC voltage control. This control is also referred to as a power angle control, and the equation for it is as follows:

$$P = \frac{|V_1|\,|V_2|}{X}\sin\theta \tag{1}$$

V_1 and V_2 are the voltage magnitudes between two nodes, θ is the difference in the phase angle and the line reactance is

X. This mathematical relationship stated that the phase angle of the voltage controls the active power.

B. Droop control

A reliable control method for the MT-HVDC system is a droop control (i.e. Voltage Droop Control (VDC)), which unlike other approach controls does not require for a communication infrastructure [19]. The VDC is a distributed control technique utilised to balance the converters' instantaneous active power. In [19] the authors clarify that the VDC requires all terminals in the MT-HVDC system to regulate their voltages via proportional control. The proportion of power that each converter shared is determined by the droop gain. The greater the power sharing for a small voltage fluctuation, the higher the droop gain, and vice versa. VDC control was developed to solve the difficulty of power sharing among converters operated in a common DC grid. The strategy of this control structure is similar to the master-slave configuration, with the exception that the power control with voltage deviation input has the droop gain added. In the FUBM model used in this paper, the VDC is classified as a control type III in the VSC control mode (see Table I and subsection II-C for more details of different control types in the VSC model in the FUBM). For this type of control, the active power (P_f) and voltage magnitude (V_{mf}) are obtained from the "from"(i.e. f) side of the FUBM model. The following is the n bus VDC mismatch equation:

$$-P^{cal}_{f(n)} + P^{set}_{f(n)} - k_{dp}\left(V^{cal}_{mf(n)} - V^{set}_{mf(n)}\right) = 0 \qquad (2)$$

In (2), the amount of the active power ($P_{f(n)}$) that flows through the VSCs depends on the magnitude of the voltage at the VSCs' *from* side, the $V_{mf(n)}$, and the parameter, k_{dp}, specifies the linear slope for the $v_{dc} - P_{f(n)}$ control. The droop characteristics of this equation, which is based on the linear power-voltage regulation is illustrated in Figure 1. One important aspect that this research highlighted was the necessity of accounting for the pre-set ramps while running short-term or day ahead optimisation.

TABLE I
TYPE OF CONTROL MODE IN VSC IN-MODEL

Mode	Constraint 1	Constraint 2	Control Type
1	θ_{sh}	v_{ac}	
2	P_f	Q_{ac}	I
3	P_f	v_{ac}	
4	v_{dc}	Q_{ac}	
5	v_{dc}	v_{ac}	II
6	$v_{dc}droop$	Q_{ac}	
7	$v_{dc}droop$	v_{ac}	III

C. The VSC's "in-model" control

VSC in-model in the FUBM is represented by a Controlled Tap-Changing Transformer (CTT) and a variable shunt susceptance (B_{eq}). The variables in the complex tap that reflect the PWM action control in the actual VSC are amplitude modulation (m'_a) and the phase shifter (θ_{sh}), which demonstrate the independent control capabilities for the active (P) and the reactive (Q) powers. Once the reactive power flow is being monitored from the "from" side, the B_{eq} will be automatically modified inside the OPF solution process to maintain the zero reactive power injection to the DC link. This process of compensating for reactive power is known as zero constraint [10]. Variable G_{sw} in the VSC "in model" represents the actual losses in the VSC, whereas the conventional P_{loss} is the variable that is adjusted in relation to the variable DC load current. The power losses must be the same in both cases. The switching losses of PWM for both conventional and VSC "in-model" are calculated as per the IEC 62751-2 standard, which employs a quadratic function. Therefore, the FUBM simulates grid isolation while maintaining the active power interchange that is identical to the traditional approach [10]. In order to keep the voltage in the DC system within the limit, the FUBM model requires that a minimum of one VSC be either type II or type III (see table I). This VSC will act as a "slack VSC," regulating the DC system's voltage [14].

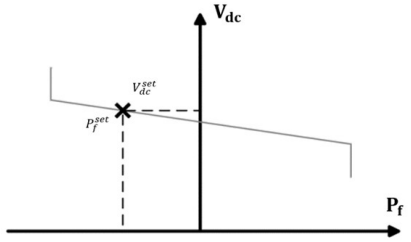

Fig. 1. Droop control ($v_{dc} - P_f$) characteristic.

III. MODEL FORMULATION

In general, the OPF is formulated as a nonlinear, nonconvex optimisation problem with the following form:

$$\min_{x,u} f(u,x) \qquad (3)$$

subject to:

$$g(u,x) = 0 \qquad (4)$$

$$h(u,x) \leq 0 \qquad (5)$$

In (3), the function "f" is defined as the objective function and "u" is the vector of m control variables; "x" is the vector of n state variables. "g" is the vector of equality constraints pertaining to the network's nodal power balance equations, and "h" is the vector inequality constraints pertaining to any physical and operational limits on the network's lines as well as other network elements (e.g., generators' power limits, transformers' tap ratios and VSCs power ratings).

A. OPF Formulation using FUBM

More explicitly for any AC power system let N be the set of all nodes and $L \subset N \times N$ the subset of all transmission lines

and $G \subset N$ be the set of all generators. The OPF problem is thus formulated as below:

$$\min_x F = \sum_{g \in G} f_g\left(P_g\right) \tag{6}$$

Subject to:

1) Equality constraint (Nodal power balance equations):

$$g_{P,k}(x) = P_k^g - P_k^d + P_k^{bus} \quad = 0, \quad k \in N \tag{7}$$
$$g_{Q,k}(x) = Q_k^g - Q_k^d + Q_k^{bus} \quad = 0, \quad k \in N \tag{8}$$

2) Inequality constraint (operational limits):

$$h_{(k,m)}^S(x) = S_{(k,m)} - L_{(k,m)}^{S(max)} \leq 0, \quad (k,m) \in L \tag{9}$$
$$x_k^{min} \leq x_k \leq x_k^{max} k \in N \tag{10}$$

For simplicity the vector "x" is used to denote both state and control variables in this formulation. An example of state variables are the nodal voltage magnitudes and in case of any control devices, for example VSCs, the control variables pertain to the variables given in Table I when modelled using the FUBM. It follows that using FUBM the injected nodal powers (real and reactive) for any devices in the system can be calculated by evaluating the admittance matrix pertaining to the FUBM general model which is given below [10].

$$Y_{fubm} = \begin{bmatrix} G_{sw} + \left(y_s + j\frac{b_c}{2} + jB_{eq}\right) & \frac{-y_s}{m_a' e^{-j\theta_{sh}}} \\ \frac{-y_s}{m_a' e^{j\theta_{sh}}} & y_s + j\frac{b_c}{2} \end{bmatrix} \tag{11}$$

For modelling the VSCs and their associated controls this admittance matrix is used to represent the VSC and is therefore used to calculate associated nodal powers (following the general form $S = V(YV)^*$) to compute the nodal real and reactive powers pertaining to the VSCs.

All VSC controls specified in Table I are therefore mathematically represented in the OPF problem as explicitly defined equality constraints as below. These are in addition to the set of equality constraints given in (7) and (8) representing nodal power balance equations.

1) Active power control:

$$g_{P_f}^n(x) = \text{Real}\left\{S_f^n(x)\right\} - P_f^{\text{set}(n)} = 0, \text{n} \in J_{sh} \cup J_{vsc} \tag{12}$$

2) Reactive power control:

$$g_{Q_t}^n(x) = \text{Imag}\left\{S_t^n(x)\right\} - Q_t^{\text{set}(n)} = 0, \text{n} \in J_{vsc} \cup J_{cct} \tag{13}$$

3) Reactive power compensation:

$$g_{Q_z}^n(x) = \text{Imag}\left\{S_f^n(x)\right\} - \text{ zero } = 0, \text{n} \in J_{vscI} \subset J_{vsc} \tag{14}$$

4) Voltage droop control:

$$g_{PV_{dp}}^n(x) = -\text{Real}\left\{S_f^n(x)\right\} + P_f^{\text{set}(n)} - k_{dp}\left(V_f^n - V_f^{\text{set}(n)}\right) = 0 \quad \text{n} \in J_{vscIII} \subset J_{vsc} \tag{15}$$

5) Converter Losses:

$$g_{G_{sw}}^n(x) = -V_f^{2(n)} G_{sw}^n + \gamma i_t^{2(n)} + \beta i_t^{2(n)} + \alpha = 0 \quad \text{n} \in J_{vsc} \tag{16}$$

Meanwhile, these equations are complemented by the following inequality constraints:

6) Line limits (including limits for the MT-HVDC DC lines):

$$h_{S_f^2}(x) = \left\{P_f^n(x)\right\}^2 + \left\{Q_f^n(x)\right\}^2 \leq \left\{L_{S_L}^n(x)\right\}^2, \text{n} \in N \tag{17}$$

$$h_{S_t^2}(x) = \left\{P_t^n(x)\right\}^2 + \left\{Q_t^n(x)\right\}^2 \leq \left\{L_{S_L}^n(x)\right\}^2, \text{n} \in N \tag{18}$$

7) Upper and lower bounds on all state variables (this includes all VSCs and all other devices):

$$x_{\min} \leq x \leq x_{\max} \tag{19}$$

It should be noted that in the above equations, the set J_{vsc} is the total set of all VSCs in the system, whereas the sets J_{sh},J_{cct} are referring to a set of Phase Shifter Transformer (PSTs) and Controlled Tap-Changing Transformer (CTTs) respectively. Subsets, $J_{vscI}, J_{vscII}, \& J_{vscIII}$ refer to the subsets of VSCs in the system that are of type I, II, or III depending on their control configurations as per Table I.

IV. Results and Discussion

The FUBM was used to model and solve the OPF for a three-terminal VSC-MTHVDC system, used to connet three Offshore Wind Farm (OWFs) and asynchronous AC grid as shown in Figure 2. The IEEE30 bus system was used to represent the asynchronous AC grid consisting of six generators, 50 transmission lines and 20 loads. The MATPOWER standard case data for this test system was used available from MATPOWER [12]. The system was simulated using MATPOWER version 7 run on MATLAB (R2021b)©using the FUBM [10]. The MT-HVDC grid and control parameters displayed in Table II were used to solve the OPF for the the proposed test system and to evaluate the impact of using different control schemes available for VSCs on steady-state operation of the test system.

TABLE II
PARAMETERS OF THE CONVERTER AND DC GRID.

Parameter	Values	
Rating VSC/DC Voltage	100MVA	200kV
Max/Min DC Voltage	1.15p.u	0.9p. u
Ma (Max/Min)	1.2	0.8
Beq (Max/Min)	0.5p. u	-0.5p. u
VSCs (rs/xs)	0.0001p.u	0.1643p.u
DC lines (rs)	0.05p.u	
VSCs loss coefficient	α = 0.0001, β = 0.015, γ = 0.2	
VSCs transmission limit	100MVA	
DCs transmission limit	200MVA	

There are four cases in this study: a) Basecase; b) DC voltage control; c) active power control; and d) droop control.

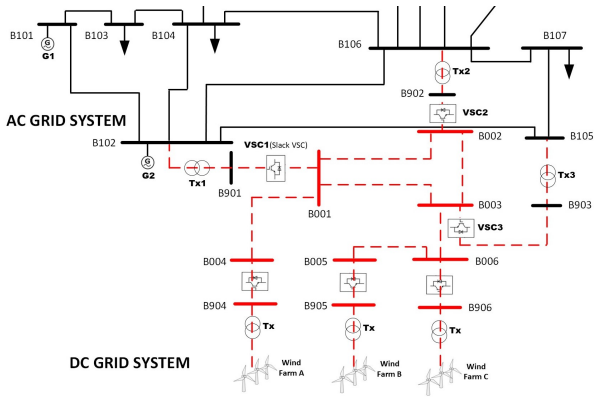

Fig. 2. MT-HVDC system

The VSC control setting for each scenario is detailed in Table III. In all cases, VSC1 is set as a "slack VSC" (i.e. reference VSC), while the other VSCs operate in accordance with their chosen control type. In cases (a),(b) and (c) the MT-HVDC system's active power was subject to the control of the VSC2 and the VSC3. As for the case (d), only VSC2 was under active power control, whilst VSC3 was controlled the reactive power.

TABLE III
SETTINGS FOR THE VSC.

No	Type of control	Converter	Type	Mode	Control constraint
1	Basecase	VSC1	II	4	Vf=1.0p. u
		VSC2	I	3	Pf = 25MW
		VSC3	I	3	Pf= 15MW
2	DC voltage control	VSC1	II	4	Vf=0. 98p.u
		VSC2	I	3	Pf = 25MW
		VSC3	I	3	Pf= 15MW
3	Active power control (+20%)	VSC1	II	4	Vf=1.0p. u
		VSC2	I	3	Pf = 30MW
		VSC3	I	3	Pf= 1MW
4	Droop control	VSC1	III	7	Vf=1.0p. u, Pf = 25MW, Kdp = -0.1
		VSC2	I	3	Pf = 25MW
		VSC3	I	2	Qt = 25MW

A. Simulation results

All simulation cases successfully converged at a single period with focused on the voltage magnitude and power flow (active and reactive), as can be seen in Table V,TableVI and Table VII. The converged time for the DC voltage control is faster compared to the other cases, which is 131.6 seconds. The system's adoption of droop control nevertheless performed the lowest convergence time at 196.47 seconds. The objective function is given in (6) as the conventional generators' total cost of generation. The convergence time and total generation cost has been given in Table IV with case (b) resulting the least operational cost.

Table V summarises the nodal voltages for the MT-HVDC link. In all cases, nodal voltages are kept within their limits with case (a) where no controls are applied in the DC link resulting the highest voltage magnitudes (in nodes 5 and 6 respectively). This is to be expected as in all other cases, at least one VSC is used to regulate the DC link voltage. In case (d) the DC link voltage depends on the active power flow control in the DC link. This indicated that the voltage decreases and increases is in direct proportion to the active power setting. In this case study, the droop control setting for this power (P_f) was set to a lower value (refer Table III).

TABLE IV
TIME CONVERGED AND GENERATION COST.

Case	Basecase	DC Voltage Control	Active power control (+20%)	Droop control
Converged (Second)	177.86	131.6	151.29	196.47
Generation cost ($/hr)	472.54	469.46	476.89	475.07

TABLE V
RESULT: VOLTAGE MAGNITUDE AND VOLTAGE ANGLE.

Bus No	Basecase		Control					
			DC Voltage		Active power (+20%)		Droop control	
	VM	VA	VM	VA	VM	VA	VM	VA
1	1	-1.357	0.98	-1.551	1	-2.376	0.954	-4.524
2	0.993	-1.357	0.973	-1.551	0.991	-2.376	0.955	-4.524
3	0.999	-1.357	0.979	-1.551	0.997	-2.376	0.963	-4.524
4	1.004	-1.357	0.984	-1.551	1.004	-2.376	0.958	-4.524
5	1.016	-1.357	0.997	-1.551	1.014	-2.376	0.981	-4.524
6	1.011	-1.357	0.992	-1.551	1.01	-2.376	0.976	-4.524

On the other hand, the Voltage Angle (VA) values in Table V were levelled off (i.e. constant) for every scenario. It is apparent that these numbers were the same for every bus in the DC grid, which is again to be expected as the FUBM models everything as notionally AC. Phase angles are therefore calculated for all nodes, including the DC link nodes, however in this case all arrive at the same number indicating that mathematically there is zero reactive power flow in the DC link and there is a coupling between DC link voltage and DC power flow within the link [14, 10].

Table VI illustrates the results for the active power flow profile in each of the branches within the MT-HVDC link for different cases. In all cases, DC power flow (PF) has been maintain within its respective limits for all branches. The DC system's active power flows (i.e. total PF from DC line 1 to DC line 3) were boosted by the active power control and the droop control, but not for cases (a) and (b). The increased active power flow for those type of controllers was around 32% and 23%. On the other hand, because the active power at the DC buses (i.e. buses 4,5 and 6) was produced by the wind farms(i.e. Wind Farm A, B and C), the active power flow across the DC line 4 to DC line 6 levelled off. This clearly shows that using additional active power flow control capabilities of VSCs, the MT-HVDC link is capable of regulating power flow from the variable wind resource at all times.

The FUBM maintains a zero reactive power flow within the DC link by activating the zero constraint seen previously in (14). It is therefore capable of accurately model the independent reactive power flow control of actual VSCs within the MT-HVDC link. As seen in table VII there is no reactive power flow within the DC branches and only VSCs' AC terminals have reactive power injections. Using FUBM, the ESO is also capable of setting VSCs to independent reactive power flow

TABLE VI
RESULT: ACTIVE POWER FLOW.

Branch	Basecase	Control			Note
		DC Voltage	Active power (+20%)	Droop control	
	PF (MW)	PF (MW)	PF (MW)	PF (MW)	
VSC1	-7.55	-7.57	-15.64	25.46	-
VSC2	25	25	30	15	-
VSC3	15	15	18	-8.16	-
DC line 1	13.56	13.57	17.96	-0.83	-
DC line 2	1.95	1.96	5.65	-16.66	-
DC line 3	-11.53	-11.52	-12.2	-15.83	-
DC line 4	-7.97	-7.97	-7.97	-7.97	WFC
DC line 5	-24.65	-24.63	-24.65	-24.62	WFB
DC line 6	10	10	10	10	WFA

control (instead of direct AC voltage control) if needed to model controls at the AC side.

TABLE VII
RESULT: REACTIVE POWER FLOW.

Branch	Basecase (MVAR)		Control					
			DC Voltage (MVAR)		Active power (+20%)- (MVAR)		Droop control (MVAR)	
	Qf	Qt	Qf	Qt	Qf	Qt	Qf	Qt
VSC1	0	-13.7	0	-13.3	0	-16.57	0	1.05
VSC2	0	-9.22	0	-3.9	0	-6.18	0	4
VSC3	0	-8.46	0	-6.32	0	-7.58	0	-25
DC line 1	0	0	0	0	0	0	0	0
DC line 2	0	0	0	0	0	0	0	0
DC line 3	0	0	0	0	0	0	0	0
DC line 4	0	0	0	0	0	0	0	0
DC line 5	0	0	0	0	0	0	0	0
DC line 6	0	0	0	0	0	0	0	0

V. CONCLUSION

The characteristic of the two types of VSC control strategies (i.e. conventional method and droop control), which had been mathematically incorporated into the OPF using the FUBM for purposes of steady-state operational planning has been successfully simulated. In all cases, the system exhibits satisfactory steady-state performance with all inequality constraints satisfied. Voltage magnitudes shown in Table V for case (d) where droop control is active for all VSCs (except for the slack VSC) show a noticeably lower magnitude of voltage. This is because of the inherent dependency of the voltage magnitude to the DC power flow within the DC link.

The maximum active power transmission occurred when active power control and droop control were implemented by 32% and 23% respectively. In all cases, the FUBM successfully modelled the operational characteristics of the DC link by: a) ensuring no reactive power flow within the DC link; and b) a coupling between voltage magnitude and the DC power flow within the DC link. This paper verifies that FUBM is a suitable model for solving OPF for the MT-DC systems used for integrating variable wind resources, and there are noticeable gains (both in operation and cost) from adopting different VSC control strategies. The ESO can use the framework presented in this paper to suitably plan an optimum operational profile for systems with large-scale converter interfaced wind integration ahead of real-time operation.

REFERENCES

[1] A. Alassi, S. Bañales, O. Ellabban, G. Adam, and C. MacIver, "Hvdc transmission: Technology review, market trends and future outlook," *Renewable and Sustainable Energy Reviews*, vol. 112, pp. 530–554, 2019.

[2] A. Raza, A. Mustafa, K. Rouzbehi, M. Jamil, S. O. Gilani, G. Abbas, U. Farooq, and M. N. Shehzad, "Optimal power flow and unified control strategy for multi-terminal hvdc systems," *IEEE Access*, vol. 7, pp. 92 642–92 650, 2019.

[3] M. Abdelwahed, H. Sindi, and E. F. El-Saadany, "Power sharing control and wind power curtailing for offshore multi-terminal vsc-hvdc transmission," in *2016 IEEE Smart Energy Grid Engineering (SEGE)*. IEEE, 2016, pp. 141–146.

[4] IRENA, "Innovation landscape brief: Supergrids," *International Renewable Energy Agency*, 2019.

[5] Y. Xue, "Modelling and control of hybrid lcc hvdc system," Ph.D. dissertation, University of Birmingham, 2016.

[6] M. A. Ikhide, "Dc line protection for multi-terminal high voltage dc (hvdc) transmission systems," Ph.D. dissertation, Staffordshire University, 2017.

[7] T. Altun, R. Madani, and A. Davoudi, "Topology-cognizant optimal power flow in multi-terminal dc grids," *IEEE Transactions on Power Systems*, vol. 36, no. 5, pp. 4588–4598, 2021.

[8] F. Capitanescu, "Critical review of recent advances and further developments in ac optimal power flow," *Electric Power Systems Research*, vol. 136, pp. 56 –68, 2016.

[9] E. Acha, P. Roncero-Sanchez, A. de la Villa-Jaen, L. M. Castro, and B. Kazemtabrizi, *VSC-FACTS-HVDC: Analysis, Modelling and Simulation in Power Grids*. Wiley, 2019.

[10] A. Alvarez-Bustos, B. Kazemtabrizi, M. Shahbazi, and E. Acha-Daza, "Universal branch model for the solution of optimal power flows in hybrid ac/dc grids," *International Journal of Electrical Power & Energy Systems*, vol. 126, p. 106543, 2021.

[11] S. S. H. Yazdi, S. H. Fathi, J. M. Monfared, and E. M. Amiri, "Optimal operation of multi terminal hvdc links connected to offshore wind farms," in *2014 11th International Conference on Electrical Engineering/Electronics, Computer, Telecommunications and Information Technology (ECTI-CON)*. IEEE, 2014, pp. 1–6.

[12] R. D. Zimmerman, C. E. Murillo-Sánchez, , and R. J. Thomas. (2020) MATPOWER: Steady-state operations, planning and analysis tools for power systems research and education. [Online]. Available: https://matpower.org/download/, https://github.com/MATPOWER/matpower

[13] A. A. Bustos and B. Kazemtabrizi, "Flexible general branch model unified power flow algorithm for future flexible ac/dc networks," in *2018 IEEE International Conference on Environment and Electrical Engineering and 2018 IEEE Industrial and Commercial Power Systems Europe (EEEIC/I&CPS Europe)*. IEEE, 2018, pp. 1–6.

[14] A. Alvarez-Bustos, "Flexible universal branch model for steady state operational analysis and optimisation of hybrid ac/dc grids," Ph.D. dissertation, Durham University, 2021.

[15] J. Li, J. Yin, Y. Guan, Z. Wang, T. Niu, H. Zhen, Z. Han, and X. Guo, "A review on topology, operating and control methods of hvdc transmission system for offshore wind farms," in *E3S Web of Conferences*, vol. 165. EDP Sciences, 2020, p. 06012.

[16] G. Stamatiou, *Converter interactions in VSC-based HVDC systems*. Chalmers Tekniska Hogskola (Sweden), 2015.

[17] A. Raza, M. Younis, Y. Liu, A. Altalbe, K. Rouzbehi, and G. Abbas, "A multi-terminal hvdc grid topology proposal for offshore wind farms," *Applied Sciences*, vol. 10, no. 5, p. 1833, 2020.

[18] Y. Zhou, L. Zhao, W.-J. Lee, Z. Zhang, and P. Wang, "Optimal power flow in hybrid ac and multi-terminal hvdc networks with offshore wind farm integration based on semidefinite programming," in *2019 IEEE Innovative Smart Grid Technologies-Asia (ISGT Asia)*. IEEE, 2019, pp. 207–212.

[19] L. Dewangan and H. J. Bahirat, "Comparison of hvdc grid control strategies," in *2017 IEEE PES Asia-Pacific Power and Energy Engineering Conference (APPEEC)*. IEEE, 2017, pp. 1–6.

[20] W. Wang, Y. Li, Y. Cao, U. Häger, and C. Rehtanz, "Adaptive droop control of vsc-mtdc system for frequency support and power sharing," *IEEE Transactions on Power Systems*, vol. 33, no. 2, pp. 1264–1274, 2017.

[21] F. Gonzalez-Longatt, "Optimal power flow in mtdc systems based on a dc-independent system operator objective," in *2015 IEEE Eindhoven PowerTech*. IEEE, 2015, pp. 1–6.